Hindawi
International Journal of Energy Research
Volume 2024, Article ID 9844646, 18 pages
https://doi.org/10.1155/2024/9844646

Research Article

Experimental Investigation and Artificial Neural Network-Based Prediction of Thermal Conductivity of Metal Oxide-Enhanced Organic Phase-Change Materials

Man Mohan[1,2,3] **Sheetal Kumar Dewangan**[1] **K. Raja Rao**[1,2] **Kwan Lee**[2] **and Byungmin Ahn**[1,4]

[1]*Department of Materials Science and Engineering, Ajou University, Suwon 16499, Republic of Korea*
[2]*Department of Electronic Materials Engineering, The University of Suwon, Hwaseong 18323, Republic of Korea*
[3]*Department of Mechanical Engineering, Rungta College of Engineering and Technology, Bhilai 490024, India*
[4]*Department of Energy Systems Research, Ajou University, Suwon 16499, Republic of Korea*

Correspondence should be addressed to Kwan Lee; kwanlee@suwon.ac.kr and Byungmin Ahn; byungmin@ajou.ac.kr

Received 29 September 2023; Revised 11 November 2023; Accepted 11 January 2024; Published 14 February 2024

Academic Editor: Hamza Faraji

This research article presents a comprehensive study on the prediction of thermal conductivity (TC) as a primary outcome for an artificial neural network (ANN) model in the context of nanoenhanced phase change materials (NEPCMs). To improve predictive accuracy and to reduce variation within the NEPCM dataset, a targeted dataset was employed, consisting exclusively of NEPCMs synthesized using paraffin wax (PW) and metal oxide nanoparticles. Unlike existing empirical models that predict TC of NEPCM without simultaneously considering multiple factors influencing it, this study integrates multiple factors, providing a more accurate prediction of NEPCM thermal conductivity. Additionally, the study explores the impact of synthesis parameters on the thermal performance of NEPCMs, focusing on the examination of factors such as the melting temperature of pure phase change material (PCM), nanoparticle size, and NEPCM composition. The thermal characterizations demonstrate outstanding thermophysical properties in NEPCMs, particularly in terms of thermal conductivity, phase change enthalpy, and thermal stability compared to their respective base PCM. An ANN TC prediction model demonstrates exceptional correlation (>99%) with reported NEPCMs, providing a reliable tool for TC forecasting in similar NEPCM categories. The backpropagation ANN model predicts NEPCM TC with a mean squared error (MSE) of 0.031124 within eight epochs. The dataset used exhibits high fit values, with R-values of 0.99825, 0.99208, and 0.9824 for training, validation, and testing, respectively. These values closely match experimentally determined TC, with less than 4% error.

1. Introduction

In 2023, phase-change materials (PCMs) are widely recognized among all materials associated with the field of renewable energy. PCMs are known as a category of energy materials that utilize the latent heat of phase transition, making them valuable thermal energy-storage substances. In the era of tough energy crises, the significance of any energy-storage material cannot be overlooked; hence, the utmost priority should be given to the development of its material characteristics to harness its utilization potential.

PCMs were introduced in the early 1900s by Alan Tower Waterman, a prominent researcher at Yale University [1]. Subsequently, significant research evolved toward understanding the thermophysical properties of PCMs. Reports in the last few years have demonstrated the continuous development of the thermophysical properties of PCMs [2–5]. Thermal energy-storage systems, which predominantly depend on solar energy, the limited availability of solar energy during daylight hours presents a significant challenge. The primary obstacle in effectively utilizing this limited time lies in the low TC of pure PCMs. This low TC

restricts the fast heat transfer necessary for efficient charging and discharging processes within thermal energy-storage devices. Consequently, the limited duration of solar energy availability cannot be effectively harnessed, as the charging and discharging rates, and overall performance of these thermal systems are adversely affected by the low TC of PCMs. Therefore, thermal conductivity emerges as the critical factor that determines the effectiveness of these energy-storage systems [6–8].

Similarly, to avoid the poor TC inherent in pure PCM, different types of nanoadditives have already been introduced as a class of materials termed nanoenhanced PCMs (NEPCMs) [9]. The class of NEPCMs is associated with diverse groups and dimensional categories of nanomaterials including 0D [10, 11], 1D [12], 2D [13], and 3D [8]. Furthermore, these particles can be subdivided into metallic, metal oxides, and carbon-derived particles, which offer distinct advantages in the formation of NEPCMs [14, 15].

In the current research scenario, similar to other conventional materials, the use of artificial intelligence (AI) to predict the thermophysical properties of advanced energy materials has also gained interest among researchers. Artificial neural network (ANN) algorithms, which have been the most common approach recently, can be employed for the accurate prediction of the TC of NEPCMs. The typical training of an ANN model requires a robust dataset; however, as some cutting-edge research is in the development phase, narrow and concise datasets for training ANNs can be scarce. To address this concern, some cases have already reported the accurate prediction of material properties with dataset restrictions. Several reports have shown the potential to utilize a limited dataset with advanced techniques like Levenberg-Marquardt [16–19], *k*-nearest neighbors (KNN) [20], automatic relevance determination [20], support vector machines [21], stochastic gradient descent [21], and adaptive neuro-fuzzy inference system [22] for effectively training the ANN model even with the lack of a comprehensive and long dataset.

Jaliliantabar [6] predicted the TC of various NEPCMs using a dataset extracted from twenty-five separate studies, each of which provided different numbers of data points. The study included particles of metal, metal oxides, carbon nanostructures, and ceramics as nanoagents, whereas the PCMs comprised both organic and inorganic materials. The input layer of the training consisted of nanoconcentrations, the temperature at which TC is measured, the phase of the NEPCM for TC measurement, the TC of the PCM, and the TC of nanomaterials. Three machine-learning methods, namely, ANN, MARS, and CART, were selected for prediction in the study. Through the collective study of all three methods, it was found that the TC of the PCM was the dominant factor among all input layers for the prediction of TC as an output layer. In addition, it was mentioned that the sample size and frequency of data at a diverse range of temperatures are critical for the number of data points. Among the three AI models, ANN performed well in terms of mean squared error (MSE) and *R*-squared values. The model training for this study was in the range of 20°C–90°C. Nevertheless, the development of new models is required to increase the pace of further research for expanding the working-temperature range of PCMs.

In another study conducted by Motahar and Sadri [17] for the prediction modeling of the TC of oxide-dispersed PCMs, an ANN model with the Levenberg-Marquardt backpropagation algorithm was trained to predict the TC of Cuo-, Al_2O_3-, TiO_2-, and SiO_2-enhanced n-octadecane. The study included one hundred and twenty-two experimental datasets extracted from the literature. The input dataset was in the range of 5°C–60°C and 0.5–12 wt% for temperature and nanoconcentration, respectively. The input layer included the temperature, mass fraction of nanoparticles, and TC of nanoparticles. The model performance was validated through MSE, mean absolute percentage error (MAPE), average absolute deviation, and correlation coefficient (*R*). The validation accuracy of data was achieved as an MSE value of 3.8059×10^{-5}, and the maximum percentage error of 2.31% was achieved for CuO-enhanced n-octadecane. Furthermore, the accuracy and performance of the network's predictions were found to have absolute errors of 0.000363 and 0.000320 W/m·K, respectively, for liquid- and solid-phase TC.

Research on the TC of NEPCM has significantly grown in the last decades; however, its exploration using AI techniques is relatively new. Consequently, the available literature related to the present study is exceptionally limited. For this reason, and to obtain a clearer understanding of the ANN-based approach, a few closely aligned and similar approaches are also included as a part of the present research.

Kumar et al. [23] developed an ANN model to predict the heat flow during the differential scanning calorimetry (DSC) of a nanoenhanced binary eutectic PCM. Dispersed multiwalled carbon nanotubes (MWCNTs) with three different mass fractions were experimentally observed in a mixture of $LiNO_3$ and NaCl for TC, chemical stability, and thermal stability. However, most of the characterization parameters of the study were not evaluated using AI, except for the heat flow prediction at different heating rates. Moreover, this study did not reveal the number of datasets for ANN modeling, which were taken from the experimental results of the study itself. During training and testing, remarkably small values of 0.000191 and 0.00505, respectively, for root mean square error were observed, which are most desirable for predicting the experimental DSC data samples accurately. In particular, the ANN model was used to predict the melting temperature and latent heat value with impressively low errors of 0.07% and 1.075%.

Kumar et al. [24] conducted experimental cum AI-based studies to predict the thermal properties of nanoencapsulated molten salt samples during DSC at different heating rates. The performance of 10^{-9} was targeted in the study by using a feedforward backpropagation algorithm. Similar to the previous study of the authors [23], DSC data prediction was the only parameter associated with ANN modeling; other characterizations were independent of AI modeling. It was reported that the trained neural network was sufficient to predict the experimental data, achieving a coefficient of determination (R^2) of 0.9985 and 0.9973 during the sampling of the training and testing datasets, respectively.

Jaliliantabar et al. [25] collected a dataset comprising twenty different nanoparticles to develop an AI-based model for the prediction of latent heat of an NEPCM. The training input layer consisted of nine neurons including a density of dispersed nanoparticles, particle size, latent heat value of PCM, density of pure PCM, and latent heat of the NEPCM. The study was based on four types of nanoparticles, namely, metal, metal oxides, carbon, and ceramic, and for all these, paraffin wax (PW) was considered the base PCM. The mixing concentration of nanoparticles was considered a dominant factor for the latent heat of the NEPCM. A multilayer perceptron (MLP) ANN was chosen to create a structure of the ANN model, and 10 neurons in the hidden layer were selected to predict the output. Notably, the dataset of paraffin-based NEPCMs was only considered to achieve the accuracy of the prediction model. The major conclusion drawn from the study is that the prediction accuracy of the output depends upon the number of data points provided for the range of the same input.

The current study is focused on experimentally exploring the TC of synthesized NEPCMs. It has two primary objectives: the first is to examine how various synthesis parameters affect thermal conductivity, and the second is to develop an AI-based model for predicting the TC of the same NEPCM. Despite growing research in this field, there is a notable absence of in-depth, AI-based prediction models specifically for NEPCMs synthesized using paraffin wax and nanoscale metal oxides. To address this issue, the present research is distinct in its approach, utilizing concise datasets comprising NEPCMs synthesized solely with the composition of paraffin wax and metal oxide nanoparticles. The significance of this specific paraffin and metal oxide-based NEPCM will be provided in the subsequent section of the manuscript.

In the present research work, our objective is to predict the TC of NEPCMs within this specific category. We acknowledge that if the AI model is trained using diverse categories of nanoparticles to synthesize NEPCM, it may lead to variations between predicted and observed values. Therefore, the primary objective of this research is to ensure the accuracy of the proposed model in predicting TC, which is why we have selected specific categories of NEPCM.

Furthermore, while various empirical models exist for TC prediction in NEPCMs, they often fail to incorporate the full spectrum of factors considered collectively in the present study [6]. Additionally, the choice of TC as the preferred outcome in our ANN-based model is driven by its direct relevance to the primary objectives of studying NEPCMs, crucial for applications like thermal energy storage, insulation, and electronics cooling. Measuring TC experimentally is often difficult and expensive, making ANN-based predictions practical and cost-effective. The availability of a reliable and significant number of TC data for validation adds to its significance in the present research. This research addresses identified gaps by offering more accurate TC predictions for paraffin wax and metal oxide-based NEPCMs, bridging discrepancies and providing a cost-effective alternative to experimental methods within this category.

2. Material Synthesis and Thermal Characterizations

As a part of the ANN training, nine distinct datasets for the TC of the NEPCM and copper oxide (CuO) nanopowders were obtained from experimental work in the present research. CuO nanoparticles were used as nanoadditives in PW for the synthesis of the NEPCM. Paraffin wax stands as a prime candidate for thermal energy storage materials due to its remarkable attributes, including thermal stability, nontoxicity, ready availability, high energy density, and its ability to maintain near-constant temperatures during phase transformations. Additionally, the exceptional thermal conductivity, chemical stability, and cost-effectiveness of nano-sized copper oxides render them an ideal choice for the widespread production of high-performance phase change materials. In combination, these factors were the driving force behind the selection of these specific materials for inclusion in the current study [26–28].

2.1. Materials. Laboratory research-grade pure PW (CAS: 8002-74-2) with three different thermal properties (Table 1) was purchased from Sigma-Aldrich and Aladdin Chemical Korea. Further, high-purity CuO nanoparticles (CAS 1317-38-0) of three different particle sizes (Table 1) and surfactant SPAN-80 (CAS:1338-43-8) were purchased from Avention and Sigma-Aldrich Korea, respectively.

2.2. NEPCM Synthesis. Apart from the literature, experimental data points for ANN training were obtained from the thermal characterization of different NEPCMs prepared by the combinations of three types of PW and nanoparticles. Additionally, the variation in the composition weight percentage of CuO particles was considered in the synthesis of NEPCMs. More specifically, the NEPCM synthesis process employs a fractional factorial approach, enabling a comprehensive exploration of key variables and efficient experimentation through robust process design to minimize the required number of experiments. In detail, the fractional factorial approach for material synthesis involves systematically varying a subset of process parameters while keeping others constant. By examining the effects of these selected factors on the material's properties, it allows for efficient experimentation and optimization. This approach enables researchers to identify critical process variables and their impact on the final product, streamlining the synthesis process [29].

The details of the NEPCM synthesis and composition are presented in Figure 1 and Table 2, respectively. The NEPCM sample preparation was carried out by direct physical mixing of CuO nanoparticles into liquid PW with the addition of SPAN-80 as a surfactant. All individual NEPCM samples were first prepared through the liquefication process of 50 gm pure paraffin in a magnetic stirring setup by keeping the temperature 5°C above the melting point of the individual PW. The process of nanoparticle addition in pure PCM involved strong magnetic stirring at 500 rpm for 50 min followed by ultrasonication at 40 kHz for 40 min. In addition to this physical mixing, SPAN-80 was used to

Table 1: Thermophysical properties of PCM and nanoadditives.

	Average particle size (nm)		TC (k_{np})* (Exp.) (W/m·K)	
CuO nanoparticles	CuO-10	10	1.064	
	CuO-40	40	1.127	
	CuO-80	80	1.069	
	Melting temperature (°C) (Experimented)		TC (W/m·K) (k_{pw})* (Exp.)	Density (ρ_{pw})* (Exp.) (kg/m^3)
PW (base PCM)	PW-10	51	0.206	799
	PW-11	51.8	0.212	778
	PW-12	62.2	0.234	874

*Measured at 25°C. Exp.: experimental values.

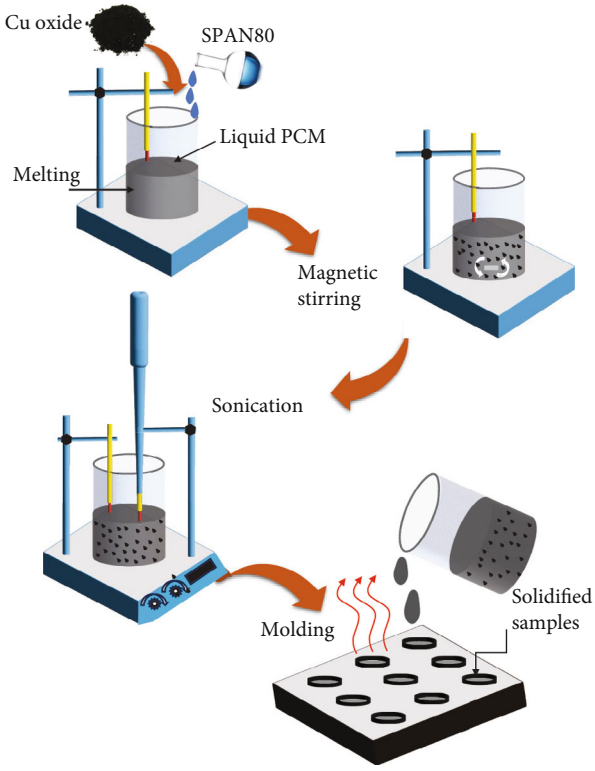

Figure 1: Schematic of the NEPCM synthesis process.

reduce the agglomeration behavior by reducing the surface tension between liquid PW and the nanoparticles. Moreover, to reduce the viscosity effect caused by temperature rise in the probe-type sonicator, the sonication process for all NEPCM samples was performed within the temperature range of 70°C–80°C. By maintaining similar procedures, nine different NEPCM samples were prepared, collected, and solidified for further characterization.

2.3. Thermal Conductivity Measurement. The LFA 457 MicroFlash (NETZCH, Germany) system was used to measure the TC of pure PW and NEPCM samples. In this setup, the thermal diffusivity of the material was measured, which was followed by the determination of its TC. All samples were prepared by a molding process to obtain a thickness of 2 mm and 10 mm sides. The schematic of the laser flash technique is provided in Figure 2, where the sample is placed in between two plates. The front surface of a plate parallel to the NEPCM sample provides heat by a short-energy light pulse, which generates a sudden and localized increase in temperature on one side of the sample. Simultaneously, the infrared detector measures the temperature of the rear face of the NEPCM.

By analyzing the temperature rise over time, it can be determined how quickly heat is being conducted through the material. The reference specimen samples were used to determine the thermal diffusivity and specific heat. The measured density of the NEPCM samples, thermal diffusivity, and specific heat were together used to calculate the TC through the following equation [30, 31]:

$$k(T) = \alpha(T).C_p(T).\rho(T), \quad (1)$$

where k is the TC (W/(m·K)), α is the thermal diffusivity (m^2/s), C_p is the specific heat (J/(kg·K)), and ρ is the bulk density (kg/m^3).

The measurement of TC has been carried out in two segments with the utmost precision. As per the instruments' calibration, the thermal diffusivity measurements were conducted with an accuracy within ±3%, while the specific heat capacity was determined with an accuracy within ±5%. Moreover, to verify the accuracy of the experimental results, twelve individual measurements were conducted for each NEPCM sample. Subsequently, the mean value was calculated and considered as the final measurement value.

2.4. Data Acquisition and ANN Modeling. The robust and concise data acquisition process for the present AI modeling and training purposes is completely based on experimental studies. The data acquisition even in previous studies exclusively relied on experimental results as the primary data source. As revealed by Table 3 and Figure 3, the data acquisition process captured one hundred sixty-nine datasets from various literature sources and the present experimentation work; out of one hundred sixty-nine data points, nine data points were contributed by the present experimentation.

Table 2: NEPCM compositions.

S. no.	NEPCM label	Pure PW melting temperature (°C)	CuO nanoparticle (Avg. particle size) (nm)	CuO in PW (wt%)	Surfactant (SPAN-80) (wt%)
1	NEPCM-1	51	10	0.3	0.3
2	NEPCM-2	51.8	40	0.3	0.3
3	NEPCM-3	62.2	80	0.3	0.3
4	NEPCM-4	51.8	10	0.6	0.6
5	NEPCM-5	62.2	40	0.6	0.6
6	NEPCM-6	51	80	0.6	0.6
7	NEPCM-7	62.2	10	0.9	0.9
8	NEPCM-8	51	40	0.9	0.9
9	NEPCM-9	51.8	80	0.9	0.9

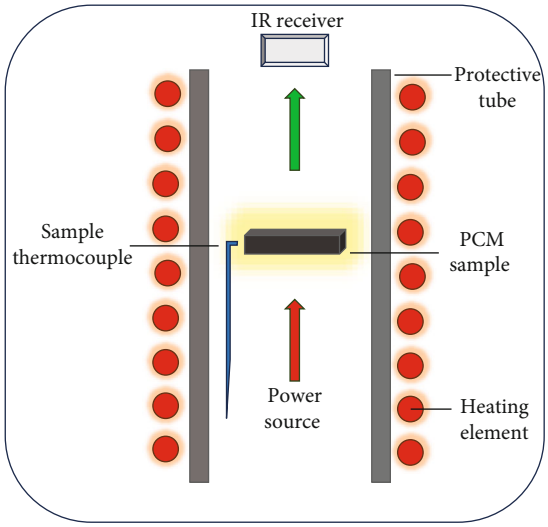

Figure 2: Schematic of the laser flash setup (TC measurement).

The dataset comprised only the class of NEPCMs synthesized exclusively by using metal oxides and PW. In particular, the dataset encompassed seven different nanoparticles (Fe_3O_4, Fe_2O_3, CuO, TiO_2, Al_2O_3, SiO_2, and ZnO_2) with PW, which is more common in such studies. This dataset was prepared by considering all significant influencing factors for the TC (k_{NEPCM}) of NEPCMs. The influencing factors are nanoparticle size (PS), melting temperature of PW (T_m), TC of PW (k_{pw}), TC of nanoparticles (k_{np}), and the temperature at which the TC of the NEPCM is measured (T_k). Moreover, the TC of the NEPCM (k_{NEPCM}) in W/m·K was considered as an outcome of the prediction model. This compiled dataset has been made available through the data availability section of the manuscript.

However, it is infrequently mentioned in the literature that the type of nanoparticle should not be considered a significant factor for such studies, which implies that diverse categories of nanoadditions can be considered collectively to form a dataset [6]. By contrast, the present study considered only metal oxides to be of particular interest and attempted to justify the model accuracy within this selection.

The compilation of a dataset encompassing a wide category of materials (including metal oxides, carbon nanotubes, organic, inorganic, refractory, and metal particles) may lead to reduced accuracy for predicting the TC of a particular subset of NEPCM. By keeping this fact in mind to predict the TC within a specific category, it is crucial to gather data exclusively from that particular category to achieve a high level of predictive accuracy. A generalized model architecture was developed as illustrated in Figure 4, which shows the input, hidden, and output layers of an ANN model used in the present modeling.

Neurons comprising each layer are interconnected through weighted links. Every neuron receives inputs and produces an output derived from stored information and the processes within the hidden layers [46]. The distribution of the dataset for training, testing, and validation purposes is 70%, 15%, and 15%, respectively. The choice for modeling involves a backpropagation neural network employing the Levenberg-Marquardt algorithm for training [16]. To achieve optimal accuracy, a 12-10-1 architecture was adopted for the modeling, and the software employed was the MATLAB 22b toolbox. The number of neurons in the hidden layers should be determined based on the problem's complexity and the amount of data available. Thus, determining the number of neurons in the hidden layers involves a trade-off between the complexity of the problem and the amount of available data. Starting with a balanced number and adjusting as needed allows you to find the right level of complexity that ensures your neural network can effectively learn the underlying patterns in the data without overfitting or underfitting. The adjustment process often involves iteratively fine-tuning the network architecture until it performs optimally on specific tasks.

Choosing to use a single hidden layer in an ANN can be a suitable option for several reasons, particularly when the problem is relatively simple or when you have limited data and computational resources. In addition, single hidden layer networks are computationally efficient and straightforward to implement. They have fewer parameters to optimize, making training faster and requiring less data. More specifically, we established a backpropagation model with a 12-10-1 architecture, comprising 12 neurons in the input layer, 10 neurons in the hidden layer, and 1 neuron in the

Table 3: Sources of the ANN training dataset.

No.	Nanoparticles	Ranges of nanoparticles (wt%)	Ranges of temperature for TC measurement	Number of data points	Reference
1.	Fe_3O_4	10–20	15	2	[32, 33]
2.	CuO	2–10	35–65	12	[34, 35]
3.	TiO_2	0.5–4	70	6	[35, 36]
4.	Al_2O_3	2.5–10	55	4	[33, 37]
5.	SiO_2	0.5–2	25	3	[26]
6.	CuO	0.3–1.2	24.7–70.5	8	[33, 35]
7.	Al_2O_3	5––10	30–60	14	[33, 38]
8.	CuO	0.1–5	25	4	[35, 39]
9.	Fe_2O_3	2–8	25	4	[40]
10.	Al_2O3	2–8	25	4	[40]
11.	ZnO	2–8	25	4	[40]
12.	SiO_2	2–8	25	8	[40]
13.	Al_2O_3	0.5–3	25–45	12	[33, 41]
14.	Al_2O_3	1	14	2	[42]
15.	TiO_2	0.5–7	15–65	41	[35, 43]
16.	TiO_2	0.25–1	25	4	[35, 44]
17.	CuO	0.25–1	25	4	[35, 44]
18.	CuO	0.3–1.2	5–30	24	[45]
19.	CuO	0.3–0.9	35	9	Present study
			Total data points	169	

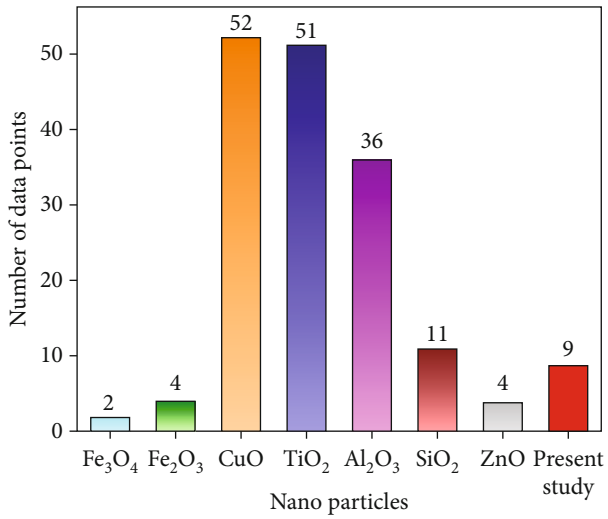

Figure 3: Data acquisition summary.

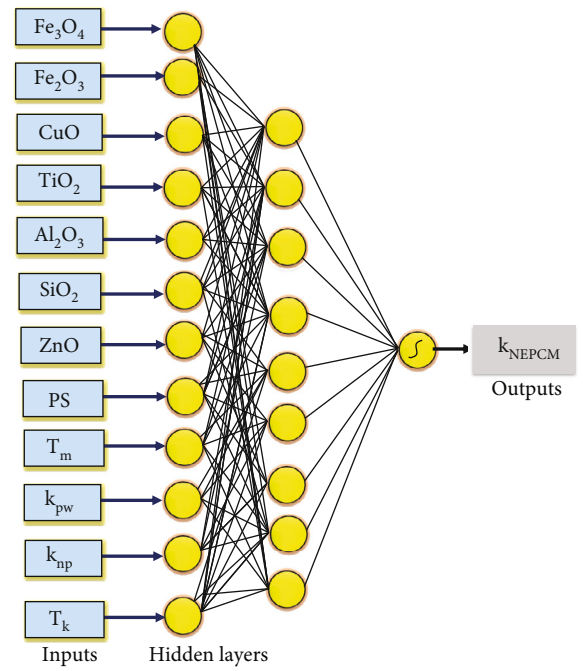

Figure 4: Architecture of the ANN model.

output layer. Specifically, the input layer functions as the entry point for ingesting raw data, while the hidden layer(s) undertakes the data processing and learning tasks. Subsequently, the output layer generates the ultimate predictions or results.

Additionally, the utmost care was taken in data acquisition for the present modeling by considering preceding research works that matched in terms of the methodology of synthesis and characterization of the NEPCMs. In this context, it is worth noting that most of the literature is primarily focused on reporting only the thermophysical properties of the NEPCMs rather than nanoadditive properties. Consequently, there is a scarcity of data on nanoadditive

Table 4: TC improvement.

NEPCM labels	TC of base PCM (k_{pw})* W/(m·K)	TC of NEPCM (k_{NEPCM})* W/(m·K)	Improved TC (%)
NEPCM-1	0.206	0.213	3.39
NEPCM-2	0.212	0.225	6.13
NEPCM-3	0.234	0.248	5.98
NEPCM-4	0.212	0.230	8.49
NEPCM-5	0.234	0.264	12.82
NEPCM-6	0.206	0.244	18.44
NEPCM-7	0.234	0.244	4.27
NEPCM-8	0.206	0.239	16.01
NEPCM-9	0.212	0.219	3.30

*Measured at 25°C.

properties, which was the primary obstacle during the data collection for the present research work. Therefore, for comprehensive dataset collection, such situations were handled with the support of other literature sources, particularly for the TC of nanoparticles.

To provide more insights into data acquisition, the dataset was compiled using available literature data. Specifically, when the melting temperature of PW was observed as a range rather than a distinct value, the average value of that range was considered. Similarly, the average values of nanoparticle size from the specified ranges were adopted. Moreover, some reports contained information only on the TC of the PCM but lacked data on the nanoparticles used; in such cases, the values of the TC of the nanoparticles were sourced from alternative references, regardless of the temperature at which the TC of the nanoparticles was measured.

3. Results and Discussion

This section presents a comprehensive analysis of TC through a comparison of the percentage improvement in TC for NEPCMs with respect to their base PCM. Additionally, the comparison between experimental and predicted thermal conductivities of NEPCMs is also presented.

3.1. Thermal Conductivity of NEPCMs. The prime objective of the present research is to develop a prediction model for the TC of NEPCMs under the effect of melting temperature and TC of PW as well as the size, TC, and composition of CuO nanoparticles. The experimental values of the TC for all the measured samples are presented in Table 4. In addition to presenting the individual TC values, a comparative analysis for all NEPCMs in terms of the reference values of thermal conductivities of pure PW (PW-10, PW-11, and PW-12) is presented in Table 4 and Figure 5.

The improved TC of the NEPCMs, in comparison to their base PCM, was analyzed among nine different samples prepared by varying the compositions. A brief discussion of TC improvement is given below. The experimental observations of the present study for the improved TC values in all NEPCM samples range from 0.213 to 0.264 W/m·K, with an enhancement in TC values ranging from 3.30 to 18.44%. As mentioned in the introduction, there has been limited research, especially regarding ANN-based TC prediction using CuO nanoparticles and paraffin wax. However, findings from the current experimental work, particularly in relation to TC, can be aligned with existing literature. This alignment is evident in the closely matching values found in the present study, which have been used to develop various ANN models for TC prediction [17].

3.1.1. PW-10 as Base PCM. A comparison of NEPCM-1, NEPCM-6, and NEPCM-8 with PW-10 revealed that all three NEPCMs exhibited improvements in TC. NEPCM-1 was found to have the lowest improvement (3.39%), followed by NEPCM-6 (15.5%) and NEPCM-8 (16.01%).

3.1.2. PW-11 as Base PCM. PW-11 was taken as a reference for NEPCM-2, NEPCM-4, and NEPCM-9, and for all these samples, improved thermal conductivities were found compared to PW-11. NEPCM-2, NEPCM-4, and NEPCM-9 demonstrated improvements of 6.13%, 8.49%, and 3.3%, respectively, compared to their base PW.

3.1.3. PW-12 as Base PCM. In the samples NEPCM-3, NEPCM-5, and NEPCM-7, which were synthesized using PW-12 as the base PCM, substantial improvements in TC were observed. NEPCM-3, NEPCM-5, and NEPCM-7 exhibited improvements of 5.98%, 12.82%, and 4.27%, respectively, compared to their base PW.

3.2. Thermal Stability and Heat Transitions. To quantify the heat exchange and thermal stability during the temperature variation of NEPCMs, DSC and thermogravimetric analysis (TGA) were, respectively, performed. The equipment details of these two experiments are provided in Table 5.

In this study, we determined the onset, endset temperatures, and latent heat using NETZSCH Proteus software. This software operates on the principle that the onset and offset temperatures are the points where extrapolated baselines intersect with tangents drawn at the inflection points to the left and right sides of the DSC curve, while the peak temperature corresponds to the highest point on the DSC curve. Apart from this, the latent heat during the melting and solidification of the NEPCM samples was calculated by integrating the area enclosed by the temperature axis within the DSC curve [47]. The phase transition heat curves and

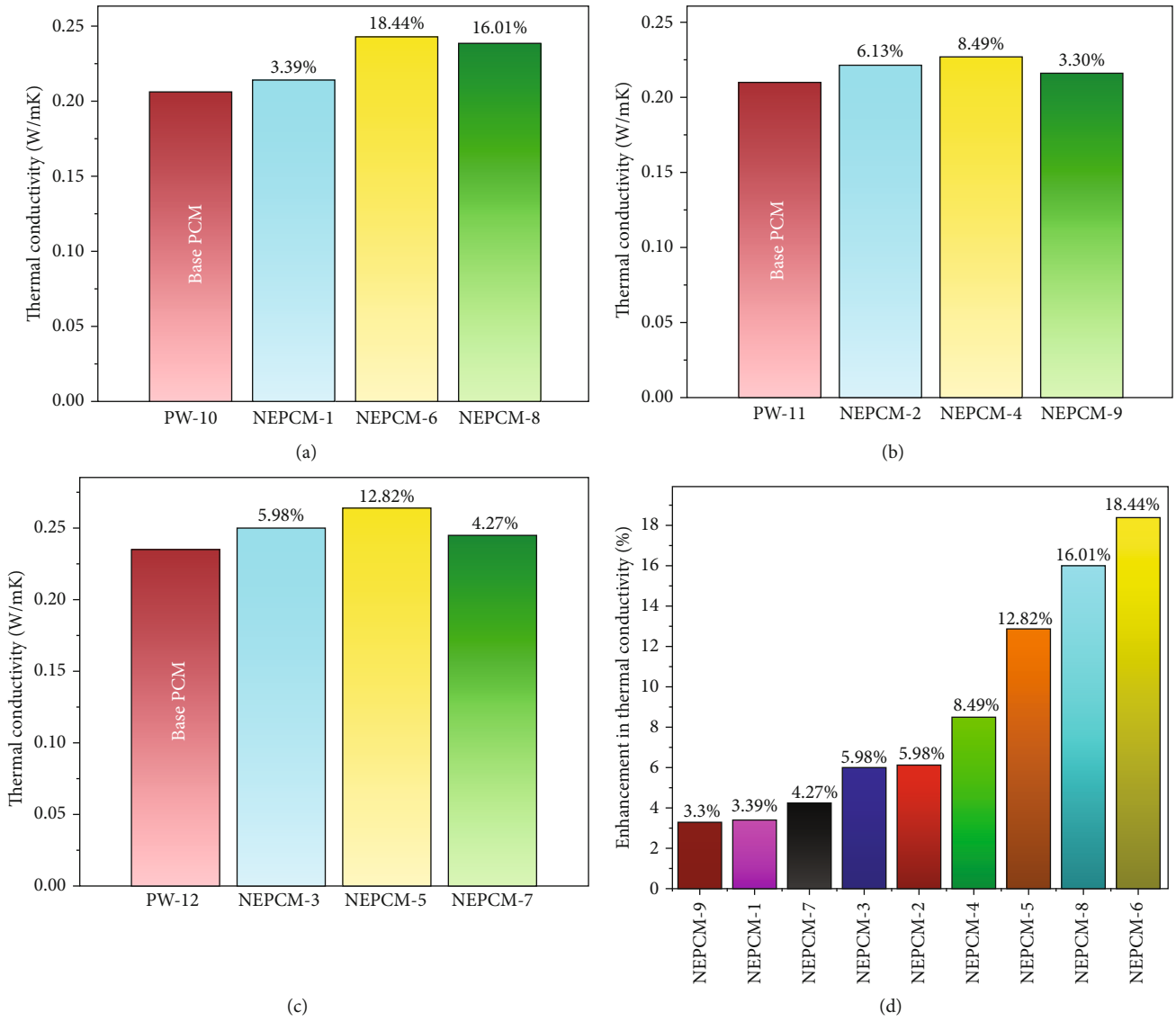

Figure 5: Percentage improvement in the TC of NEPCMs compared to the respective base PCMs.

Table 5: Experimentation and equipment details (DSC and TGA).

	Equipment model	Heating/cooling rate	Purge atmosphere	Observation range
DSC	DSC200F3Maia (NETZSCH)	5°C/min	Nitrogen	15°C–85°C
TGA	NETZSCH STA 449F3	10°C/min	Nitrogen	28°C–650°C

mass decomposition curves during the phase change of pure PW are collectively presented in Figures 6(a) and 6(b), respectively, while both the patterns for all NEPCM samples are shown in Figures 7 and 8.

The in-depth analysis of DSC curves as tabulated in Table 6 reveals that the majority of NEPCM samples showed an upward trend in melting enthalpy. The incorporation of nanoparticles into phase change materials (PCMs) enhances their latent heat capacity through increasing the number of nucleation sites for phase change, allowing a greater portion of the PCM to participate in the phase transition. Additionally, nanoparticles improve thermal conductivity, ensuring more effective heat transfer and leading to alterations in their phase transition behavior [45]. However, among a few NEPCM samples, the maximum reduction in melting enthalpy of ~0.9% was observed for NEPCM-9. Decrements in melting and solidification enthalpies are rarely encountered, and their impact can be neglected because of the nominal change in the latent heat capacities of NEPCMs. All the fluctuations of melting and solidification enthalpy presented in Table 6 were observed with respect to the base PCM of all individual NEPCMs.

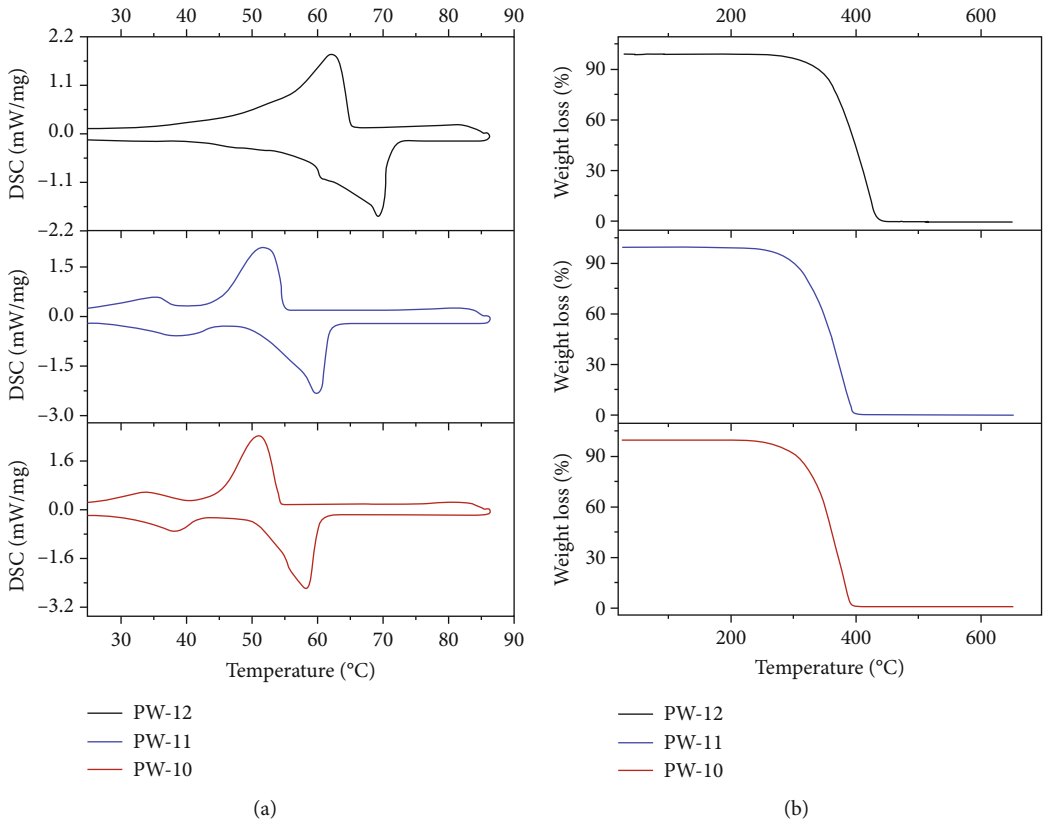

Figure 6: Thermal behavior: DSC and TGA of pure PW.

For instance, all three NEPCM samples synthesized from PW-12 exhibited a continuous rise in melting enthalpy (NEPCM-3, NEPCM-5, and NEPCM-7). This increased melting enthalpy can be observed to have a linear relation with the increasing size of the incorporated nanoparticles. Among all NEPCMs, the highest improvement of 9% in melting enthalpy was observed for NEPCM-3. This highest improvement can be correlated with the high melting temperature of PW-12 as the base PCM for NEPCM-3. Similarly, the most substantial improvement in solidification enthalpy was observed to be ~4.5% for NEPCM-5 with respect to its base PCM. This improved solidification enthalpy was the most noticeable improvement across all the NEPCMs.

Additionally, Figure 8 illustrates the mass decomposition of the synthesized NEPCM samples. This pattern of thermal decomposition confirms the potential for their application within the degradation onset temperature for each individual NEPCM. The degradation onset temperature justifies the temperature range within which these NEPCMs can be effectively used without undergoing undesirable changes in their properties due to thermal degradation. It has also been observed that all the NEPCMs displayed lower degradation onset temperatures relative to their corresponding base PCMs. This phenomenon shows the impact of metal oxide nanoparticles, which enhance phase transition efficiency by lowering the energy barrier and improving thermal conductivity.

As noted in prior research studies, interactions between the nanoparticles and the PCM at the nanoscale influence thermodynamic properties, including intermolecular forces, resulting in alterations in the energy needed for phase transition [48, 49].

3.3. Prediction through ANN. The MSE holds prime importance in achieving precise prediction outcomes. Hence, it was utilized as the key criterion for model selection. Despite numerous attempts resulting in accurate predictions, this study ultimately opted for the most favorable outcome, which was the TC of the NEPCMs. For regression tasks, MSE measures the average squared error or absolute difference between predicted and actual values, respectively. The lower MSE values indicate better predictive accuracy. In addition, R-squared is a metric for regression models that indicates the proportion of the variance in the dependent variable that is explained by the model. So, a higher R-squared value is desirable to achieve a high degree of accuracy.

Figure 9(a) illustrates a histogram showcasing the distribution of discrepancies between target and predicted values following the training of a feedforward neural network. These disparities can assume negative values, signifying the extent of deviation between projected and desired values. The histogram comprises vertical bars and termed bins, which categorize the overall range of errors into 20 more manageable segments. The y-axis indicates the count of samples falling within each bin. For instance, the bin centered around an error of 0.02103 exhibits a height close to ~60 for the training dataset and values between 60 and 70 for the validation and test datasets. The x-axis represents

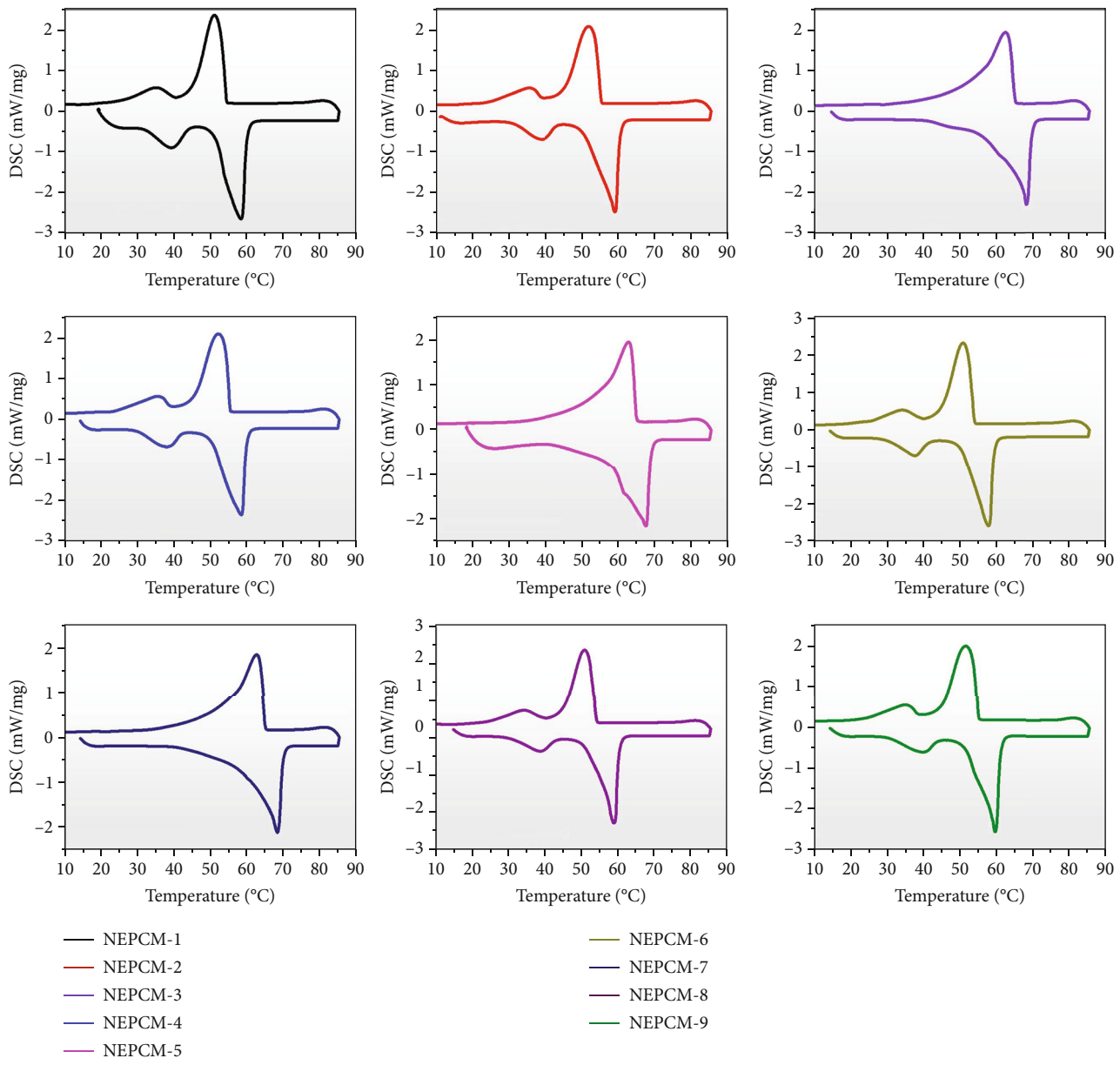

Figure 7: Thermal behavior: DSC analysis of NEPCMs.

the zero-error line for reference. In this context, the zero-error point coincides with the bin centered at 0.02103.

During the training process, many trials are performed in order to find the best ANN structure that has the least mean squared error (MSE). As the significance of the validation performance (Figure 9(b)) is based on the MSE, which is the most important factor in choosing a suitable model, the best result has been chosen and presented in the work. Since such kind of a trial is made by hundreds of iterations on an error and trial basis.

Thus, during the training, validation, and testing, Eqs. (2)–(4), respectively, were calculated by the models that are as follows.

$$\text{Output} \cong 1 \times \text{Target} + 0.0077, \tag{2}$$

$$\text{Output} \cong 0.85 \times \text{Target} + 0.045, \tag{3}$$

$$\text{Output} \cong 1 \times \text{Target} + 0.046, \tag{4}$$

where output is the model's final result, and the target is the actual experimental value.

The choice of the 12-10-1 architecture was driven by the minimal MSE value to achieve the highest accuracy [50]. As depicted in Figure 9(b), the 12-10-1 ANN model demonstrated its superior validation performance, reaching an MSE of 0.031124 after eight epochs. Furthermore, the correlation of the selected model was demonstrated with an overall R-value of 0.99368. The predictions from the ANN predictive model can be visualized and compared with the experimental findings to assess their level of agreement. As depicted in Figure 10, the experimental outcomes of the

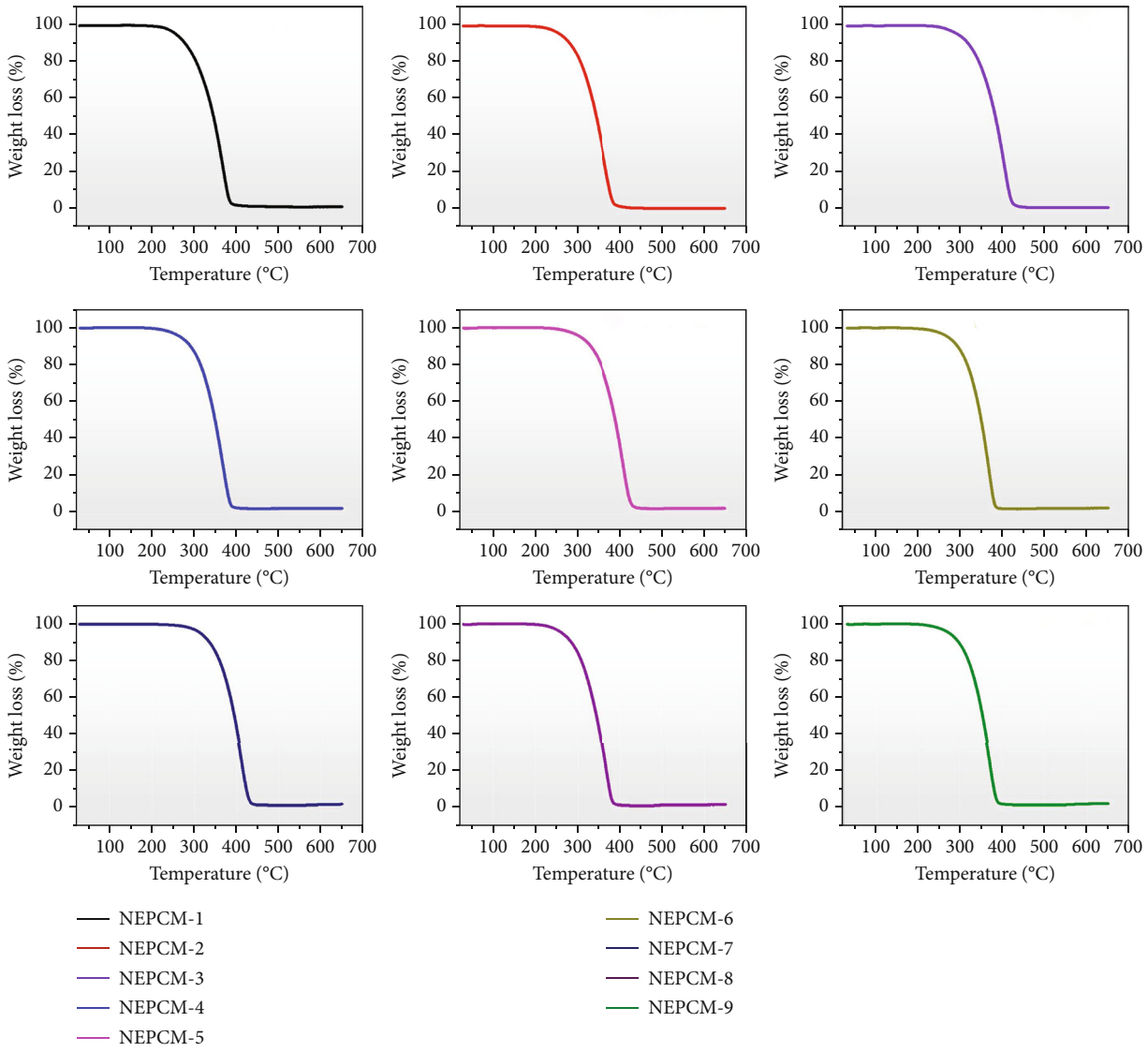

Figure 8: Mass decomposition: TGA of NEPCMs.

present study closely align with the anticipated results, as evidenced by the R-values (correlation coefficient) of 0.99825, 0.9828, and 0.99208 for training, testing, and validation, respectively, with an overall R-value of 0.99368 (Figures 10(a)–10(d)).

In addition, to validate the choice of the LM algorithm, the simulation has also been formed by using the same model by altering the LM algorithm which is, namely, Bayesian regularization backpropagation and scaled conjugate gradient backpropagation algorithm. It is found that $R = 0.98133$, 6.0134×10^{-5} for Bayesian regularization and $R = 0.96736$ and MSE = 0.06773 for the scaled conjugate gradient. Thus, the result shows a better prediction as compared to the other two algorithms.

Moreover, plotting the experimental results and the output of the ANN model together revealed an exact match of the TC (k_{NEPCM}) predictions. Detailed results of the projected TC are provided in the data availability section of the manuscript, indicating an overall absolute error of ~3.83%.

The TC projection shown in Figure 11 exhibits an outstanding resemblance to the experimental curve, showcasing the practicality of the ANN model in predicting the TC of NEPCMs to identify a new class of NEPCMs. This underscores the reliability and consistency of the ANN model as a robust approach for TC prediction in alloy systems.

3.4. Validation of Model. In order to validate the accuracy of the model employed in the present study, a comparison has been made in Table 7 among different models, including the present study by adopting different algorithms (LM-BP, Bayesian regularization backpropagation, and scaled conjugate gradient backpropagation) by evaluating the MSE, R, and R^2 values.

Through this comparison, it can be concluded that in the context of a present ANN model for predicting TC in NEPCMs, key considerations include the utilization of advanced regularization techniques, custom loss functions, and interpretability tools to capture complex and nuanced correlations in the data. These advanced techniques enable

Table 6: Phase transition enthalpy of NEPCMs and pure PW.

	NEPCM-1	NEPCM-2	NEPCM-3	NEPCM-4	NEPCM-5	NEPCM-6	NEPCM-7	NEPCM-8	NEPCM-9	PW-10 (base PCM)	PW-11 (base PCM)	PW-12 (base PCM)
Melting enthalpy (J/g)	155	150.9	215	149.6	210.8	151.8	205	147.9	147.8	152.4	149.2	197.1
Change in melting enthalpy (%)	+1.7	+1.1	+9.0	+0.2	+6.9	−0.39	+4.0	−0.29	−0.9	Base PCM	Base PCM	Base PCM
Freezing enthalpy (J/g)	149.9	146.2	212	146.6	212.3	148.5	204.5	144.6	144.2	145.8	144.7	203
Change in solidification enthalpy (%)	+2.8	+1.03	+4.4	+1.3	+4.5	+1.8	+0.7	−0.8	−0.3	Base PCM	Base PCM	Base PCM

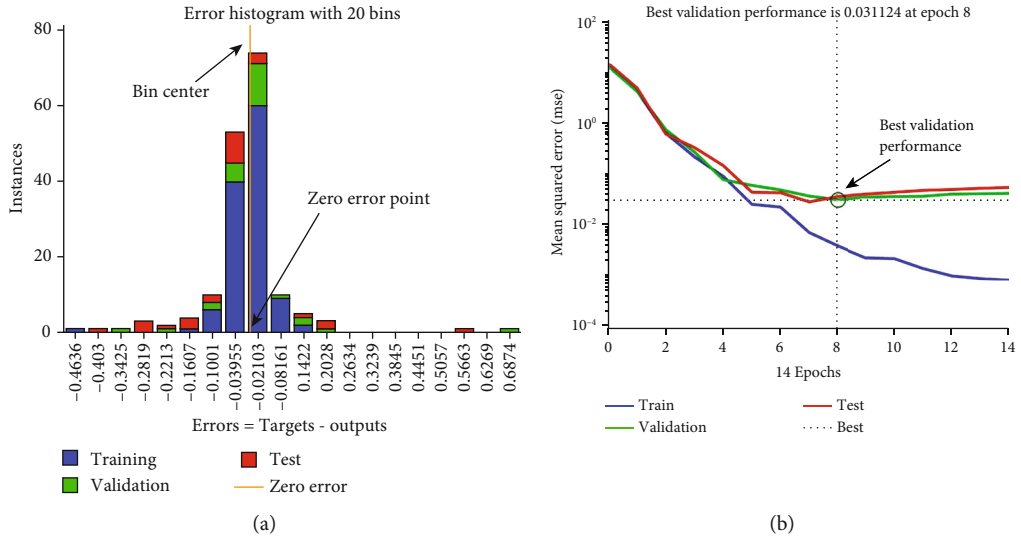

Figure 9: (a) Error histogram and (b) MSE error for the proposed 12-10-1 ANN model.

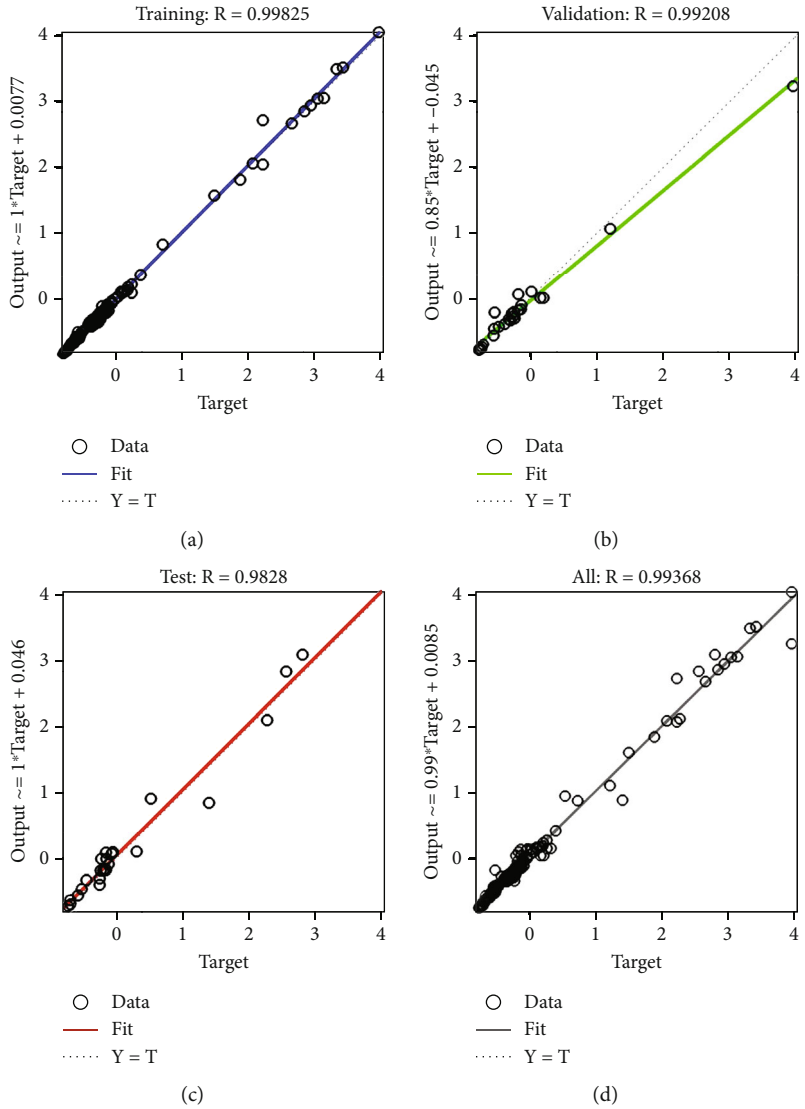

Figure 10: Correlation of the dataset with (a) training, (b) validation, (c) test, and (d) overall for the 12-10-1 ANN model.

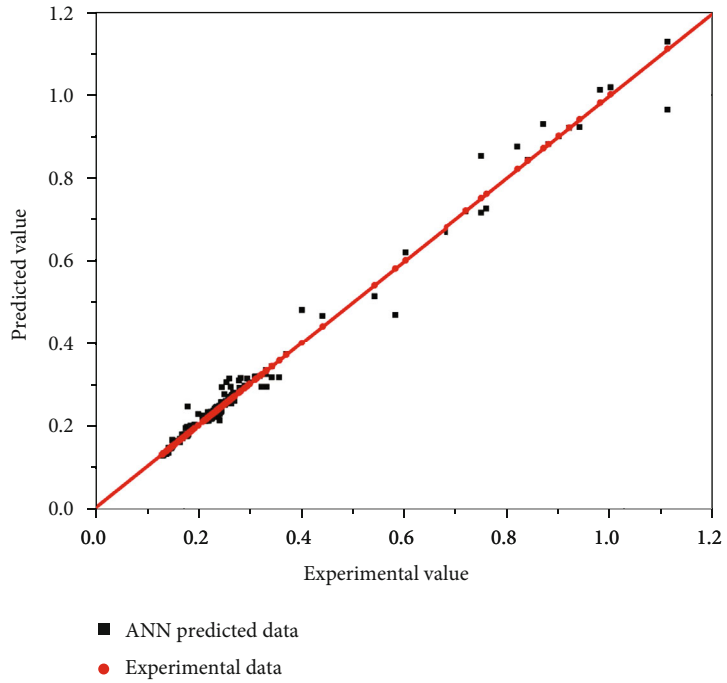

Figure 11: Comparison of experimental and ANN-predicted densities.

Table 7: Comparison of different ANN model accuracy.

Materials	Model used	Accuracy level	Ref.
Miscellaneous PCM+ metal oxide nanoparticles	Levenberg-Marquardt backpropagation algorithm	MSE = 1.3512×10^{-5} $R = 0.999964948$	[17]
Paraffin wax + metal oxide nanoparticles	Huber regression method	MSE = 0.971172 $R^2 = 0.998$	[21]
	KNN ($K = 3$)	MSE = 0.41809 $R^2 = 0.999$	
	SVM (RBF kernel)	$R^2 = 0.999$ MSE = 0.000016	
Paraffin wax + metal oxide and carbon-based nanoparticles	MARS CART ANN	$R^2 = 0.93$ $R^2 = 0.93$ $R^2 = 0.96$	[6]
Paraffin wax + metal oxide nanoparticles	ANN (Levenberg-Marquardt backpropagation)	$R = 0.99368$ MSE = 0.031124	Present work
	ANN (Bayesian regularization backpropagation)	$R = 0.98133$ MSE = 6.0134×10^{-5}	
	ANN (scaled conjugate gradient backpropagation)	$R = 0.96736$ MSE = 0.06773	

the model to better understand and predict TC, even when dealing with limited data and intricate relationships between input variables, ultimately enhancing the model's accuracy and its ability to uncover meaningful correlations in NEPCMs.

4. Limitations and Challenges

The conclusions drawn from this research are valuable, but it is essential to consider the limitations of the ANN prediction model used:

(i) *Data Requirements*. The neural network model typically requires a large amount of training data to perform well. In cases where data is limited, ANNs may overfit, making them unreliable for prediction. Despite the model's success in this study, the limited dataset could potentially affect its reliability in broader applications. Additionally, challenges include the quality of thermal conductivity data, which can affect the model's performance

(ii) *Overfitting Mitigation*. It is mentioned that the used ANN model was optimized with several iterations, and the learning algorithm was carefully selected. However, in practice, overfitting can still be a concern, especially if the dataset is small and not diverse. The reliability of the model may vary in situations with significantly different data

(iii) *Scope Limitations*. The study is limited to specific parameters, such as the size of nanoparticles, a specific temperature range of measurement, PCM melting temperature, thermophysical properties of materials, and specific materials (metal oxide with paraffin wax). This makes the model's applicability outside of these constraints uncertain. In real-world applications with different materials or conditions, the model may not perform as well

(iv) *Data Preprocessing Complexity*. Data preprocessing can be intricate, involving the cleaning and preparation of data for training. Developing complex ANN models can be challenging and making them interpretable can be an issue

(v) *Generalization Requirement and Data Diversity*. Achieving generalization to different materials and conditions is crucial for the model's utility. The diversity of materials, data imbalance, and the need for domain knowledge further complicate the modeling process

(vi) *Data Handling and Fine-Tuning*. Addressing these challenges may involve rigorous data handling and model fine-tuning to ensure accurate predictions of thermal conductivity

(vii) *Model Optimization*. The 12-10-1 model used in this study was optimized with several iterations and the proper selection of the learning algorithm to overcome these challenges and produce the best results

In summary, while the ANN prediction model demonstrated strong correlation and reliability within the defined scope of the research, its limitations related to data requirements, overfitting, and limited scope should be considered when applying it in broader contexts or with different parameters. Researchers and users should be cautious about extrapolating the model's performance beyond the specific conditions tested in this study.

5. Conclusions

A significant part of the present investigation has been accomplished by the synthesis and thermal characterization of different NEPCMs. The thermal characterization revealed excellent thermophysical properties of NEPCMs over their base PCMs. Three major thermophysical properties, namely, TC, melting, and solidification enthalpies, were extensively compared for improving the thermal performance of NEPCMs. Furthermore, an ANN model was developed to predict the TC of NEPCMs through a comparison with literature data. Some key conclusions drawn from this study are as follows:

(i) The incorporation of CuO nanoparticles along with varying PCM composition and melting temperature contributes significantly to TC improvement, with enhancements ranging from 3.4% to 18.44%

(ii) Adding larger nanoparticles to a low-melting-temperature PCM significantly increases TC compared to NEPCMs with high-melting-temperature base PCMs. Higher nanoparticle concentrations do not consistently yield the highest TC enhancement

(iii) In two different NEPCMs with the same nanoparticle size, a minor reduction in the melting temperature of the base PCM (1.5%) combined with comparatively low concentrations of nanoparticles can result in a substantial enhancement in TC up to 15.14%

(iv) Similar to melting enthalpy, the most substantial improvement of 4.5% in solidification enthalpy is observed for one of the NEPCMs having the highest melting temperature for its base PCM

(v) A backpropagation ANN model is established, which successfully predicts the TC of NEPCMs with an MSE of 0.031124 at eight epochs. It is found that the used dataset has fitted R-values 0.99825, 0.99208, and 0.9824 for training, validation, and testing, respectively, in the prediction of TC using the ANN model, which is well correlated with the experimentally determined TC with less than 4% error

(vi) The ANN prediction model for TC has an outstanding correlation (>99%) with the reported NEPCMs, which could be used as an effective and readily available tool for determining the TC of NEPCMs according to their application

6. Future Scope and Recommendations

To enhance the applicability of AI models for predicting thermal conductivity in NEPCMs, future research should expand the model's training dataset to include a wider range of nanomaterials commonly used in NEPCM synthesis and with using different prediction models. This diversification equips the model to predict thermal conductivity across various NEPCM materials, enhancing its versatility and making it a valuable tool for a comprehensive understanding of these materials. In the current study, the authors have addressed the challenge of collecting extensive thermal conductivity data for different NEPCMs under varying synthesis conditions by developing an efficient ANN prediction model. This model can serve as a valuable supporting tool for optimizing the composition of NEPCMs, particularly in cases where collecting large experimental datasets is challenging, contributing to advancements in the field. Additionally, the correlation between AI modeling and thermal conductivity is evident in how these models enable industries to optimize

processes, reduce energy consumption, and improve material design. This, in turn, leads to more sustainable and cost-effective practices. The applications of AI in predicting TC have far-reaching implications in various sectors, making them a valuable tool for research, development, and manufacturing.

Nomenclature

0D: Zero-dimensional
1D: One-dimensional
2D: Two-dimensional
3D: Three-dimensional
AI: Artificial intelligence
Al_2O_3: Aluminum oxide
EG: Ethylene glycol
ANN: Artificial neural network
CART: Classification and regression trees
C_p: Specific heat (J/(kg·K)
CuO: Cupric oxide
DSC: Differential scanning calorimetry
Fe_3O_4: Magnetite
K: Thermal conductivity (W/m·K)
kHz: Kilohertz
LM-BP: Levenberg-Marquardt backpropagation
MARS: Multivariate adaptive regression
MAPE: Mean absolute percentage error
MASE: Mean absolute percentage error
MWCNT: Multiwalled carbon nanotubes
MSE: Mean squared error
MLP: Multilayer perceptron
m^3: Volume
NaCl: Sodium chloride
NEPCMs: Nanoenhanced phase-change materials
nm: Nanometer
PW: Paraffin wax
PCM: Phase-change materials
PS: Nanoparticle size
R: Correlation coefficient
R^2: Coefficient of determination
SAE: Society of Automotive Engineers
SPAN-80: Sorbitan monooleate
SiO_2: Silicon dioxide
rpm: Revolutions per minute
TGA: Thermogravimetric analysis
TC: Thermal conductivity
TiO_2: Titanium dioxide
T_k: Temperature at which the TC of the NEPCM is measured
%: Percentage
ρ: Bulk density (kg/m^3)
α: Thermal diffusivity (m^2/s)
°C: Degree Celsius.

Data Availability

The data used in this study are part of further research. To access the data, please contact the authors with a reasonable request. The raw data can be accessed through the following link: https://github.com/HEAresearch/Thermalconductivity_PCM.git.

Conflicts of Interest

The authors declare that they have no conflicts of interest.

Acknowledgments

This research was supported by the Basic Science Research Program through the National Research Foundation of Korea (NRF) funded by the Ministry of Education (RS-2023-00249523).

References

[1] M. Mhadhbi, "Introductory chapter: phase change material," in *Phase Change Materials and Their Applications*, pp. 1–6, IntechOpen, 2018.

[2] L. Han, X. Zhang, J. Ji, and K. Ma, "Research progress on the influence of nano-additives on phase change materials," *Journal of Energy Storage*, vol. 55, article 105807, 2022.

[3] S. Tan and X. Zhang, "Progress of research on phase change energy storage materials in their thermal conductivity," *Journal of Energy Storage*, vol. 61, article 106772, 2023.

[4] S. C. Lin and H. H. Al-Kayiem, "Evaluation of copper nanoparticles - paraffin wax compositions for solar thermal energy storage," *Solar Energy*, vol. 132, pp. 267–278, 2016.

[5] V. P. Kalbande, G. Fating, M. Mohan, K. Rambhad, and A. K. Sinha, "Experimental and theoretical study for suitability of hybrid nano enhanced phase change material for thermal energy storage applications," *Journal of Energy Storage*, vol. 51, article 104431, 2022.

[6] F. Jaliliantabar, "Thermal conductivity prediction of nano enhanced phase change materials:a comparative machine learning approach," *Journal of Energy Storage*, vol. 46, article 103633, 2022.

[7] B. Eanest Jebasingh and A. Valan Arasu, "A detailed review on heat transfer rate, supercooling, thermal stability and reliability of nanoparticle dispersed organic phase change material for low-temperature applications," *Materials Today Energy*, vol. 16, article 100408, 2020.

[8] O. Abou Saima and A. A. Abdel-Rehim, "Experimental and numerical analysis for the size, charging and discharging characteristics of a phase changing material as a thermal energy storage," *Journal of Energy Storage*, vol. 58, article 106228, 2023.

[9] Q. Wang, L. Yang, and J. Song, "Preparation, thermal conductivity, and applications of nano–enhanced phase change materials (NEPCMs) in solar heat collection: a review," *Journal of Energy Storage*, vol. 63, article 107047, 2023.

[10] R. Hidki, L. E. Moutaouakil, M. Boukendil, Z. Charqui, Z. Zrikem, and A. Abdelbaki, "Natural convection heat transfer analysis of a nano-encapsulated phase change material (NEPCM) confined in a porous square chamber with two heat sources," *Journal of Energy Storage*, vol. 73, article 108924, 2023.

[11] H. Faraji, Ç. Yıldız, A. Arshad, M. Arıcı, K. Choukairy, and M. E. Alami, "Passive thermal management strategy for cooling multiple portable electronic components: hybrid nanoparticles enhanced phase change materials as an

innovative solution," *Journal of Energy Storage*, vol. 70, article 108087, 2023.

[12] J. L. Zeng, F. R. Zhu, S. B. Yu et al., "Effects of copper nanowires on the properties of an organic phase change material," *Solar Energy Materials and Solar Cells*, vol. 105, pp. 174–178, 2012.

[13] W. Ren, L. Cao, and D. Zhang, "Composite phase change material based on reduced graphene oxide/expanded graphite aerogel with improved thermal properties and shape-stability," *International Journal of Energy Research*, vol. 44, no. 1, pp. 242–256, 2020.

[14] B. M. S. Punniakodi and R. Senthil, "Recent developments in nano-enhanced phase change materials for solar thermal storage," *Solar Energy Materials and Solar Cells*, vol. 238, article 111629, 2022.

[15] Z. Jiang, X. Li, Y. Jin et al., "Particle technology in the formulation and fabrication of thermal energy storage materials," *Chemie-Ingenieur-Technik*, vol. 95, no. 1-2, pp. 40–58, 2023.

[16] S. K. Dewangan, A. Sharma, H. Lee, V. Kumar, and B. Ahn, "Prediction of nanoindentation creep behavior of tungsten-containing high entropy alloys using artificial neural network trained with Levenberg–Marquardt algorithm," *Journal of Alloys and Compounds*, vol. 958, article 170359, 2023.

[17] S. Motahar and S. Sadri, "Applying artificial neural networks to predict the enhanced thermal conductivity of a phase change material with dispersed oxide nanoparticles," *International Journal of Energy Research*, vol. 45, no. 10, pp. 15092–15109, 2021.

[18] S. K. Dewangan, S. Samal, and V. Kumar, "Microstructure exploration and an artificial neural network approach for hardness prediction in AlCrFeMnNiWx high-entropy alloys," *Journal of Alloys and Compounds*, vol. 823, article 153766, 2020.

[19] S. Fidan, H. Oktay, S. Polat, and S. Ozturk, "An artificial neural network model to predict the thermal properties of concrete using different neurons and activation functions," *Advances in Materials Science and Engineering*, vol. 2019, Article ID 3831813, 13 pages, 2019.

[20] Y. Gao, I. M. T. A. Shigidi, M. A. Ali, R. Z. Homod, and M. R. Safaei, "Thermophysical properties prediction of carbon-based nano-enhanced phase change material's using various machine learning methods," *Journal of Taiwan Institute of Chemical Engineering*, vol. 148, article 104662, 2023.

[21] M. Bakouri, H. S. Sultan, S. Samad, H. Togun, and M. Goodarzi, "Predicting thermophysical properties enhancement of metal-based phase change materials using various machine learning algorithms," *Journal of Taiwan Institute of Chemical Engineering*, vol. 148, article 104934, 2023.

[22] A. G. Olabi, A. A. Abdelghafar, H. M. Maghrabie et al., "Application of artificial intelligence for prediction, optimization, and control of thermal energy storage systems," *Thermal Science and Engineering Progress*, vol. 39, article 101730, 2023.

[23] K. Ravi Kumar, K. R. Balasubramanian, B. S. Jinshah, and N. Abhishek, "Experimental analysis and neural network model of MWCNTs enhanced phase change materials," *International Journal of Thermophysics*, vol. 43, no. 1, pp. 1–31, 2022.

[24] K. R. Kumar, K. R. Balasubramanian, G. P. Kumar, C. Bharat Kumar, and M. M. Cheepu, "Experimental investigation of nano-encapsulated molten salt for medium-temperature thermal storage systems and modeling of neural networks," *International Journal of Thermophysics*, vol. 43, no. 9, pp. 1–30, 2022.

[25] F. Jaliliantabar, R. Mamat, and S. Kumarasamy, "Latent heat prediction of nano enhanced phase change material by ANN method," *Energy Engineering*, vol. 119, no. 3, pp. 847–861, 2022.

[26] P. Manoj Kumar, K. Mylsamy, and P. T. Saravanakumar, "Experimental investigations on thermal properties of nano-SiO2/paraffin phase change material (PCM) for solar thermal energy storage applications," *Energy Sources, Part A: Recovery, Utilization, and Environmental Effects*, vol. 42, no. 19, pp. 2420–2433, 2020.

[27] S. Sharma, L. Micheli, W. Chang, A. A. Tahir, K. S. Reddy, and T. K. Mallick, "Nano-enhanced phase change material for thermal management of BICPV," *Applied Energy*, vol. 208, pp. 719–733, 2017.

[28] K. Y. Leong, M. R. A. Rahman, and B. A. Gurunathan, "Nano-enhanced phase change materials: a review of thermo-physical properties, applications and challenges," *Journal of Energy Storage*, vol. 21, pp. 18–31, 2019.

[29] G. Dwivedi and M. P. Sharma, "Application of Box-Behnken design in optimization of biodiesel yield from pongamia oil and its stability analysis," *Fuel*, vol. 145, pp. 256–262, 2015.

[30] NETZSCH, "Analyzing and testing, Laser flash appar. LFA 457 MicroFlash," 2023, https://analyzing-testing.netzsch.com/en/products/thermal-diffusivity-and-conductivity/lfa-457-microflash.

[31] B. Cheng, B. Lane, J. Whiting, and K. Chou, "A combined experimental-numerical method to evaluate powder thermal properties in laser powder bed fusion," *Journal of Manufacturing Science and Engineering*, vol. 140, pp. 1–8, 2018.

[32] N. Şahan, M. Fois, and H. Paksoy, "Improving thermal conductivity phase change materials–a study of paraffin nanomagnetite composites," *Solar Energy Materials and Solar Cells*, vol. 137, pp. 61–67, 2015.

[33] J. Wang, Y. Li, D. Zheng, H. Mikulčić, M. Vujanović, and B. Sundén, "Preparation and thermophysical property analysis of nanocomposite phase change materials for energy storage," *Renewable and Sustainable Energy Reviews*, vol. 151, article 111541, 2021.

[34] S. Jesumathy, M. Udayakumar, and S. Suresh, "Experimental study of enhanced heat transfer by addition of CuO nanoparticle," *Heat and Mass Transfer*, vol. 48, no. 6, pp. 965–978, 2012.

[35] L. Sahota and G. N. Tiwari, "Exergoeconomic and enviroeconomic analyses of hybrid double slope solar still loaded with nanofluids," *Energy Conversion and Management*, vol. 148, pp. 413–430, 2017.

[36] S. Sami and N. Etesami, "Improving thermal characteristics and stability of phase change material containing TiO_2 nanoparticles after thermal cycles for energy storage," *Applied Thermal Engineering*, vol. 124, pp. 346–352, 2017.

[37] M. Nourani, N. Hamdami, J. Keramat, A. Moheb, and M. Shahedi, "Thermal behavior of paraffin-nano- Al_2O_3 stabilized by sodium stearoyl lactylate as a stable phase change material with high thermal conductivity," *Renewable Energy*, vol. 88, pp. 474–482, 2016.

[38] C. J. Ho and J. Y. Gao, "Preparation and thermophysical properties of nanoparticle-in-paraffin emulsion as phase change material," *International Communications in Heat and Mass Transfer*, vol. 36, no. 5, pp. 467–470, 2009.

[39] M. George, A. K. Pandey, N. Abd Rahim, V. V. Tyagi, S. Shahabuddin, and R. Saidur, "A novel polyaniline (PANI)/paraffin wax nano composite phase change material: superior transition heat storage capacity, thermal conductivity and thermal reliability," *Solar Energy*, vol. 204, pp. 448–458, 2020.

[40] A. Babapoor and G. Karimi, "Thermal properties measurement and heat storage analysis of paraffinnanoparticles composites phase change material: comparison and optimization," *Applied Thermal Engineering*, vol. 90, pp. 945–951, 2015.

[41] M. T. Chaichan and H. A. Kazem, "Single slope solar distillator productivity improvement using phase change material and Al_2O_3 nanoparticle," *Solar Energy*, vol. 164, pp. 370–381, 2018.

[42] L. Colla, L. Fedele, S. Mancin, L. Danza, and O. Manca, "Nano-PCMs for enhanced energy storage and passive cooling applications," *Applied Thermal Engineering*, vol. 110, pp. 584–589, 2017.

[43] J. Wang, H. Xie, Z. Guo, L. Guan, and Y. Li, "Improved thermal properties of paraffin wax by the addition of TiO_2 nanoparticles," *Applied Thermal Engineering*, vol. 73, no. 2, pp. 1541–1547, 2014.

[44] S. Harikrishnan, K. Deepak, and S. Kalaiselvam, "Thermal energy storage behavior of composite using hybrid nanomaterials as PCM for solar heating systems," *Journal of Thermal Analysis and Calorimetry*, vol. 115, no. 2, pp. 1563–1571, 2014.

[45] J. Wang, Y. Li, Y. Wang, L. Yang, X. Kong, and B. Sundén, "Experimental investigation of heat transfer performance of a heat pipe combined with thermal energy storage materials of CuO-paraffin nanocomposites," *Solar Energy*, vol. 211, pp. 928–937, 2020.

[46] S. K. Dewangan, S. Samal, and V. Kumar, "Development of an ANN-based generalized model for hardness prediction of SPSed AlCoCrCuFeMnNiW containing high entropy alloys," *Materials Today Communications*, vol. 27, article 102356, 2021.

[47] S. A. Memon, "Phase change materials integrated in building walls: a state of the art review," *Renewable and Sustainable Energy Reviews*, vol. 31, pp. 870–906, 2014.

[48] A. Anand, V. Srivastava, S. Singh, A. Shukla, A. K. Choubey, and A. Sharma, "Development of nano-enhanced phase change materials using manganese dioxide nanoparticles obtained through green synthesis," *Energy Storage*, vol. 4, no. 5, 2022.

[49] T. P. Teng and C. C. Yu, "Characteristics of phase-change materials containing oxide nano-additives for thermal storage," *Nanoscale Research Letters*, vol. 7, no. 1, pp. 1–10, 2012.

[50] R. Jain, S. K. Dewangan, V. Kumar, and S. Samal, "Artificial neural network approach for microhardness prediction of eight component FeCoNiCrMnVAlNb eutectic high entropy alloys," *Material Science Engineering A*, vol. 797, article 140059, 2020.